

Article

A Portable Direct Methanol Fuel Cell Power Station for Long-Term Internet of Things Applications

Chung-Jen Chou ^{1,*} , Shyh-Biau Jiang ¹, Tse-Liang Yeh ², Li-Duan Tsai ³, Ku-Yen Kang ³ and Ching-Jung Liu ³

¹ Institute of Opto-Mechatronics Engineering, National Central University, Taoyuan City 32001, Taiwan; sbjiang@viewmove.com

² Institute of Mechanical Engineering, National Central University, Taoyuan City 32001, Taiwan; tlyeh@cc.ncu.edu.tw

³ Material and Chemical Research Laboratories (MCL), Industrial Technology Research Institute (ITRI), B77, 195, Sec. 4, Chung Hsing Rd. Chutung, Hsingchu City 31057, Taiwan; LiDuanTsai@itri.org.tw (L.-D.T.); KYK@itri.org.tw (K.-Y.K.); mo@itri.org.tw (C.-J.L.)

* Correspondence: petpoku@gmail.com; Tel.: +886-3-4227151 (ext. 34387)

Received: 22 April 2020; Accepted: 7 July 2020; Published: 9 July 2020



Abstract: With regard to the best electro-chemical efficiency of an active direct methanol fuel cell (DMFC), the stacks and their balance of plant (BOP) are complex to build and operate. The yield of making the large-scale stacks is difficult to improve. Therefore, a portable power station made of multiple simpler planar type stack modules with only appropriate semi-active BOPs was developed. A planar stack and its miniature BOP components are integrated into a semi-active DMFC stack module for easy production, assembly, and operation. An improved energy management system is designed to control multiple DMFC stack modules in parallel to enhance its power-generation capacity and stability so that the portability, environmental tolerance, and long-term durability become comparable to that of the active systems. A prototype of the power station was tested for 3600 h in an actual outdoor environment through winter and summer. Its performance and maintenance events are analyzed to validate its stability and durability. Throughout the test, it maintained the daily average of 3.3 W power generation with peak output driving capability of 12 W suitable for Internet of Things (IoT) applications.

Keywords: direct methanol fuel cell; multi stacks; portable power; energy management system; Internet of Things; long-term; in-field test

1. Introduction

Developing intelligent services to cover remote areas, Internet of Things (IoT) networks need to be deployed in places such as farms, forest, outlying islands, infrastructure piping, etc., where there is no electricity power grid. Acquiring power supply has always been a problem. Thus, this has led to demands for long-term reliable power supplies [1]. Secondary batteries are commonly used on IoT equipment. However, due to limited energy storage, connection to a power source for charging is still necessary for long operations. In addition to engine-driven generators, two types of power sources, namely, the energy-harvesting sources [2–5] and fuel cells (FCs) [6,7], can be used to charge. When installing energy-harvesting device, we need to consider the availability of the natural energy source and location suitability. Moreover, to meet steady demand, large enough capacity of the secondary batteries is needed to buffer the inherently uncontrollable variations in the natural energy resource [8–10]. Therefore, these power supplies are difficult to be portable. On the other hand, FCs demonstrate stable power generation needing relatively low battery buffering capacity. They can be installed quickly with the ability to work for a long time.

The FCs generate power by electrochemical reactions of different fuel types in different reaction modes. These are: polymer electrolyte fuel cell (PEMFC), direct methanol fuel cell (DMFC), direct formic acid fuel cell (DFAFC), direct ethanol fuel cell (DEFC), and solid oxide fuel cell (SOFC) [11–13]. Using liquid fuel, a DMFC has a higher fuel volume energy density so that the system is lightweight, easy to replenish, safe, and can be operated at room temperature. Therefore, DMFCs are suitable candidates portable power supplies for emergency deployments and IoT applications [14–16].

Facilitating an optimal environment for efficient electrochemical reactions, the balance of plant (BOP) of a DMFC can be an aggressive active type or a sub-optimal passive type. A passive DMFC maintains balance during electrochemical reactions without external forces. The architecture is simple. However, its electro-chemical efficiency is sensitive to the environment, the power generation is unstable, and the system durability is poor [17,18]. In an active DMFC, BOP components are installed to regulate the conditions for optimal reactions so that high power generation efficiency, stability, environmental tolerance, and long-term durability can be maximized for marketability. Therefore, the majority of DMFC products on the market are the active type [19]. Nevertheless, active DMFCs are disadvantaged by the complexity of the stack assembly process [20], the excessive number of BOP components, and complex in-system piping. Therefore, active DMFCs have low manufacturing yield, are difficult to miniaturize, and difficult to repair [21,22]. To ensure optimal operating conditions, the complexity of an active DMFC system is necessary. On the other hand, for simplicity, the passive DMFCs may be stable for only limited power output and operation time. However, for portability and long-term power generation reliability, a marketable semi-active DMFC design needs to be weighed between complexity and optimization. To address the complexity shortcomings of the active DMFCs, modularization would be one of the primary solutions. Additionally, several studies on the modularization of FCs, including stack modular design, combination of multiple stack modules, and control management of multiple stack modules have been proposed [23–27].

While a modularized stack can be individually installed, put in operation and serviced conveniently, there are great advantages to having multiple stack modules functioning collectively to increase power capacity, and to enhance the durability with added redundancies. Following this strategy, a novel architecture and control of the DMFC power station is developed with specifications suitable for IoT applications. Simplifying the system architecture, the functionalities of BOP components in the active DMFCs were reviewed. Only the necessary components were miniaturized and integrated onto the passive DMFC to form a compact semi-active DMFC stack module. The mechanism of a power station was reworked with much simplified wiring and piping to accept convenient multi-stack module plug-ins and to be operated collectively by one energy management system (EMS). Space for a larger fuel tank can, therefore, be made available for a longer period before refueling.

Although managing the fuel, heat and water of a DMFC for efficiency and durability is complicated and difficult compared with other types of FC [22,28], integrating controls of the electromechanical system with the EMS to accommodate the load demand can make improvements. Simultaneous controls of the limited BOP components in multiple DMFC stacks can maintain proper operating conditions of the semi-active DMFC power station effectively such that its environmental tolerance, endurance, and power generation stability of the system can approach that of an active DMFC. In verifying our new design, long-term evaluation of the system performance, the regulation of operating conditions by the BOP components, and the changes in stack characteristics is essential [29,30]. Therefore, a prototype of our power station was tested for 3600 h in actual outdoor environments throughout winter and summer under different weathers, temperatures, and humidity to verify its suitability for IoT applications in the field.

2. Design of a Modular Semi-Active Direct Methanol Fuel Cell (DMFC) Power Station

A DMFC power station contains two major systems. One is the DMFC stack system for electrochemical reactions, and the other is the EMS to control the reaction conditions and energy balance.

2.1. DMFC Stack System

The DMFC stack system consists of a fuel-cell stack, BOP components and piping for air or liquid delivery. The DMFC stack is the core for the electrochemical reaction, and the BOP components assist in maintaining appropriate reaction conditions, supplying appropriate amount of reactants, and discharging by-products.

Figure 1 is a comparison of the BOP components in an active and our semi-active DMFC stack system. The whole block diagram represents an active system architecture, while the semi-active system consists of only a fuel tank plus the members encircled by the red dashed line. All four members enclosed in the dashed line can be constructed using only miniaturized components such that the complex active DMFC stack system can be slimmed down to a compact stack module. In addition, the semi-active DMFC stack module is made of only two separate sets of planar stack and flow field plates without the need for precise channel alignment and pressurized spacing, thereby greatly reducing the production difficulties. With a sufficient air contact area, an air blower instead of an air pump is enough and one piezoelectric dosing pump is enough to supply fuel. Thus, miniature BOPs can be integrated into the stack module.

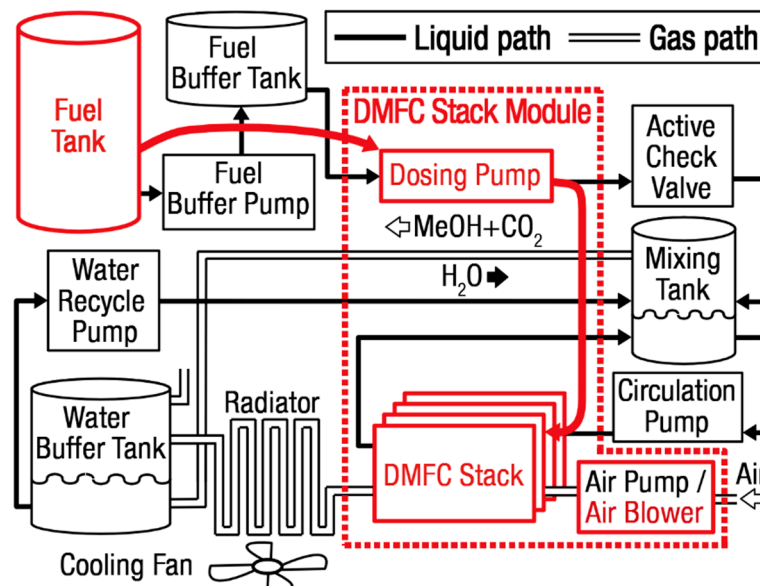


Figure 1. Comparing full balance of plant (BOP) components in an active direct methanol fuel cell (DMFC) stack system with that of a semi-active system marked in red, where a DMFC stack module is enclosed by the red dashed line.

Simplifying the active architecture, the semi-active stack module does not have active temperature, humidity control, fuel buffer tank, nor check valve, therefore, supporting measures are needed. The feedback control on the fuel-supplying dosing pump was implemented to compensate the influence of changing the fuel level height on the flow rate. Fuel tank was relocated below the DMFC stack modules to prevent leakage due to either gravity or pressure imbalances. Due to the passive water recovery mechanism, the air supply flow rate was reduced and the reaction temperature was also decreased from the electrochemical optimum of 75 °C to 45 °C to reduce excessive water evaporative loss.

Figure 2 shows the photo of the semi-active DMFC stack module proposed. The stack module has a sandwich structure, with planar DMFC stacks on both sides with the metal electrodes protruding on the top. The flow field plate is in the middle with two air blowers on the right edge blowing air supplying oxygen. The fuel dosing pump is mounted at the lower right corner with an inlet connected to the fuel tank through a hose. It has membrane electrode assembly (MEA) of 61.6 cm², 8 cells series,

operating at 2.8 V to generate 1 W nominally. Its dimension is $120 \times 60 \times 15 \text{ mm}^3$ and it weighs less than 200 g.

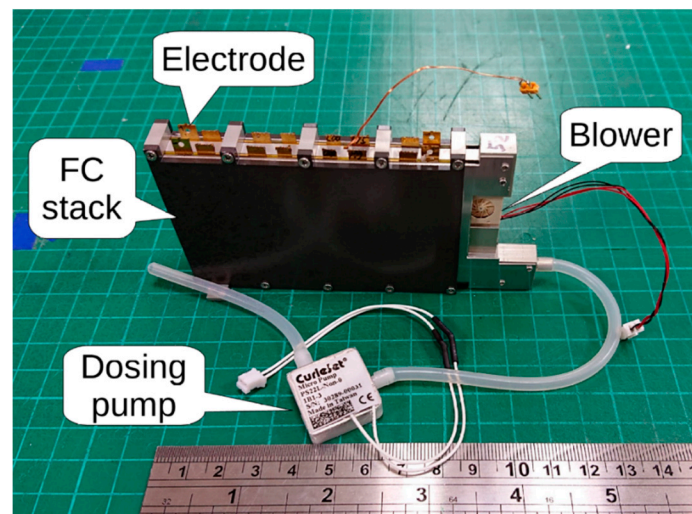


Figure 2. Semi-active DMFC stack module.

2.2. Energy Management System (EMS)

Figure 3 is the functional block diagram of the semi-active DMFC power station. The DMFC stack system is located on the top consisting of a fuel tank and a set of four DMFC stack modules. The lower half is the function block diagram of the EMS controlling the collective operating conditions and status report communication.

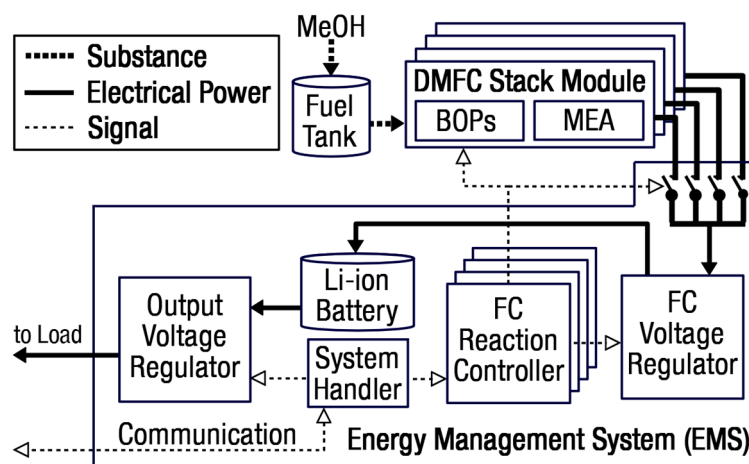


Figure 3. Semi-active DMFC power station functional block diagram.

The EMS has a system handler at the core of the multiple sets of FC reaction controller. FC reaction controllers coordinate the BOPs in the stack modules to work, while the FC voltage regulators keep the modules properly loaded to maintain the electrochemical reactions and manage the energy storage into the battery. The switches between the stack modules and the regulator determine the operating mode of the corresponding module, whether it is offline for maintenance or online in parallel power generation. Li-ion batteries act as energy buffer between generation and output demand. The output voltage regulator serves the output demand. There is a core supervisor monitoring the status of the batteries to control the inhibition of the power generation and the output power drive so that batteries are protected from over charge or discharge.

When DMFC stacks are activated, they can be switched online and offline independently, and their working voltages and currents can change rapidly as a variable energy source. In order to have their electricity output connected in parallel for stable power generation, the dynamic energy management control is designed to maintain the stability of their reaction voltages to the setpoint V_{sp} by the FC voltage regulator. Given the characteristics of the MEA, the generator current estimator estimates I_{es} as the target current to draw from stacks. It also adjusts the current estimate based on the error between the present FC voltage V_{FC} and the setpoint voltage V_{sp} so that V_{FC} converges to V_{sp} . In the inner loop, the current feedback controller measures the actual output current I_o and quickly adjusts the direct current to direct current (DC/DC) converter so that I_o tracks I_{es} . Meanwhile, all electricity generated, namely I_o drawn from the stack, gets pumped into the battery for storage.

The right side of Figure 4 shows the output voltage regulator taking energy from the Li-ion battery to drive the output demand. Wherein, the output converter is a boost DC/DC converter controlled by the system handler. When enabled, it draws from the battery voltage to drive the output voltage. The output would be turned off when disabled to prevent over drawing on the batteries. An eFuse module which prevents excessive output current and reversed current against load variation improves the reliability of the power station.

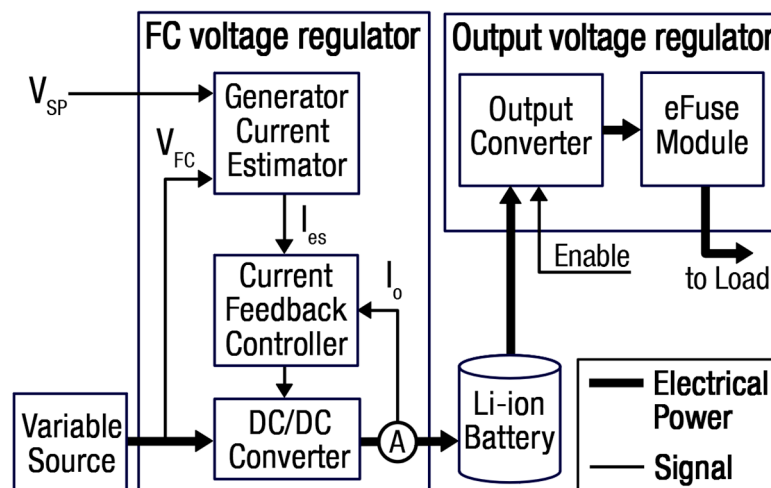


Figure 4. The fuel-cell (FC) voltage regulator and the output voltage regulator block diagram.

The electrochemical reaction conditions of the DMFC stack modules are maintained by their individual BOPs under the coordinated control of the FC reaction controller as shown in Figure 5a. The reaction voltage calculator determines the appropriate stack reaction voltage setpoint V_{sp} , based on the ambient conditions, the stack temperature and the characteristics of the DMFC stack module, for the FC voltage regulator to follow. The fuel supply calculator determines the fuel consumption to control the dosing pumps to replenish according to the sensor-less approach equation, Equation (1). Assuming only a portion of the fuel consumed by the DMFC stack module is effectively converted into electricity I_{FC} and the rest is the temperature dependent crossover, thus derived the fuel consumption estimator according to sensing measurements.

$$S = K_T \int_0^{\Delta t} I_{FC} \cdot dt + K_c \cdot \Delta t \quad (1)$$

where S is the total fuel consumption over a given period Δt , K_T is the fuel consumption coefficient resulting in effective power generation represented by the DMFC output current I_{FC} , and K_c is the fuel consumption rate resulting in the crossover. Both K_T and K_c coefficients are determined from the MEA size, the stack module characteristics, and the ambient temperature. The backbone of the controls is to maintain the proper heat generation for temperature management. The fuel consumption

is estimated by Equation (1) to determine the appropriate fuel supply to maintain, to increase, or to decrease current operating temperature.

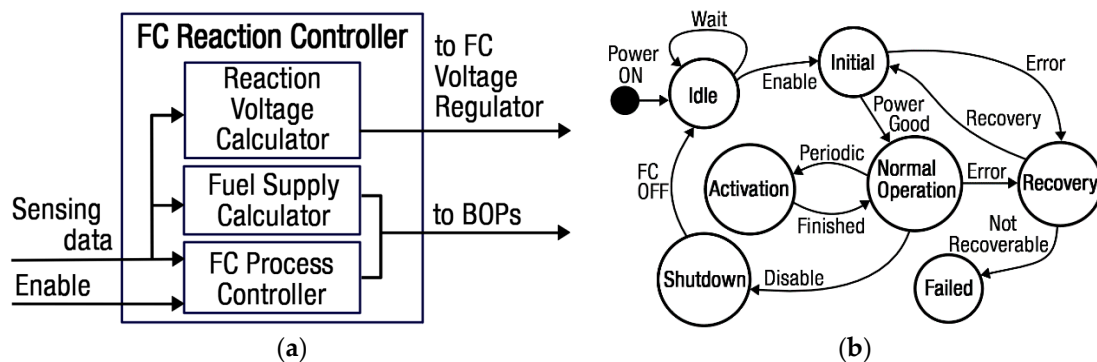


Figure 5. (a) Functional block diagram of an FC reaction controller; (b) the state machine of the FC process controller.

Figure 5b illustrates the state machine of the FC process controller explaining the logic behind the controls. When the power station is turned on, it first enters the idle state. When the enable signal is triggered, it enters the initial state that the controller controls the fuel supply and stack voltages to increase the stack temperature progressively. When the initial process ends, the state enters the normal operation state. If it yields an abnormal result, then the process enters the recovery state. In the normal operation state, the stack module continues to generate power, perform self-tests, and periodically switches to the activation state. If an error occurs, then the process switches to the recovery state. When the disable command is received, it switches to the shutdown state for safe turn off. While operating in the recovery state, the process attempts to resolve the stack problem. If it succeeds, the controller returns to the initial state to restart or the controller enters the fail state to stop any operations on this stack. In the activation state, the process blocks the stack current, stops supplying oxygen and waits 60 s. Afterwards, the controller returns to normal operation to generate electricity again. This process refreshes the MEAs, the reaction efficiency of which deteriorated after long usage.

The system handler of the EMS sets the system operating modes according to the commands received from the communication as well as the Li-ion battery voltage monitored. The power output is disabled when the battery voltage is less than 3.5 V, and it will be reactivated only until the voltage exceeds 3.7 V. The station power generating is enabled when the battery voltage falls below 3.8 V and will be disabled when the charged voltage rises above 4.1 V. The overall power balance of whole DMFC power station is described by Equation (2)

$$P_{BAT} = P_{FC} \cdot \eta_{Reg} - P_{Load} \cdot D_{Load} - P_{EMS} \quad (2)$$

where P_{BAT} denotes the power charging the batteries, P_{FC} is the total FC power generation, η_{Reg} is the efficiency of the FC voltage regulator, P_{Load} is the power station output power to the external load, D_{Load} is the working duty of the external load, and P_{EMS} is the power consumption of EMS. With the battery buffering and the output voltage regulator, P_{Load} is designed up to 12 W exceeding P_{FC} and to be suitable to drive IoT applications.

2.3. DMFC Power Station

Figure 6a shows the front view of the portable DMFC power station. Its dimension is $26 \times 22 \times 22$ cm³, and it weighs approximately 2 kg. A fuel injection port is located at the left of the front cover, a heat sink was attached on the right side cover, and vent holes were provided on the top and side for good air circulation.

Figure 6b shows the rear view of the inside. A 4 L fuel tank approximately half of the height of the power station was placed at the bottom providing 1.5 to 2 kWh energy generation capacity to last longer than 20 days of continuous operation. DMFC stack module sockets to accept four stack modules were placed on the upper left side. The number of modules to be plugged in can be determined by the power demand of the targeted application. The EMS control board is located on the upper right. The Li-ion batteries are placed at the right front of the fuel tank. The installation and replacement of the DMFC stack modules are simple and quick, connecting the dosing pump to the fuel tank with a hose, plugging electronic signal and power cables into the corresponding EMS sockets, and it is done. The power station is easy to assemble, to maintain, and portable. We conducted a long-term field test to demonstrate its feasibility for IoT applications in outdoor environments.

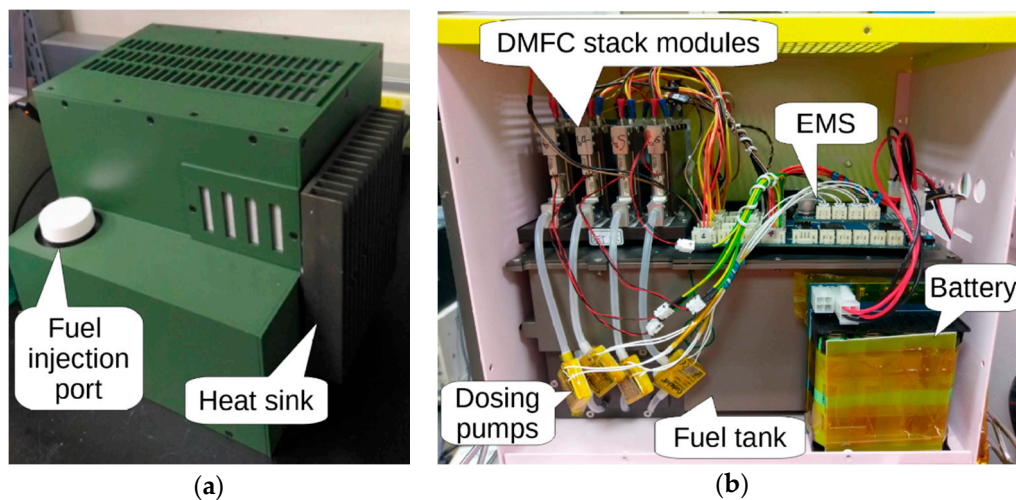


Figure 6. Portable DMFC power station. (a) Front view; (b) rear view internal configuration

3. Experimental Setup

To verify the viability for field applications, the ability of long-term stable electric power generation in a real outdoor environment is a key issue. The experimental test was performed over half a year, beginning in winter and ending in summer, thus covering a variety of weather conditions with wide temperature and humidity variations. From the test, the degradation of components was assessed, and the controls, the fueling, and the maintenance strategies was further refined.

Figure 7a depicts the experimental environment and instrument configuration. The power station was placed in a small outdoor rain-proof cabinet on the roof of a building to simulate an actual field environment. A supervising personal computer was placed indoors for remote status check and data logging. Figure 7b shows the inside of the cabinet where the power station was placed in the test and the dummy load acting as its power demand. Throughout the test, supervising the system for debugging as well as validation purposes, the data recorded are the voltage, current, temperature of the stack modules, the Li-ion battery, the outdoor ambient, and the inside of the cabinet. The performance data were accumulated to one sample per minute for analysis.

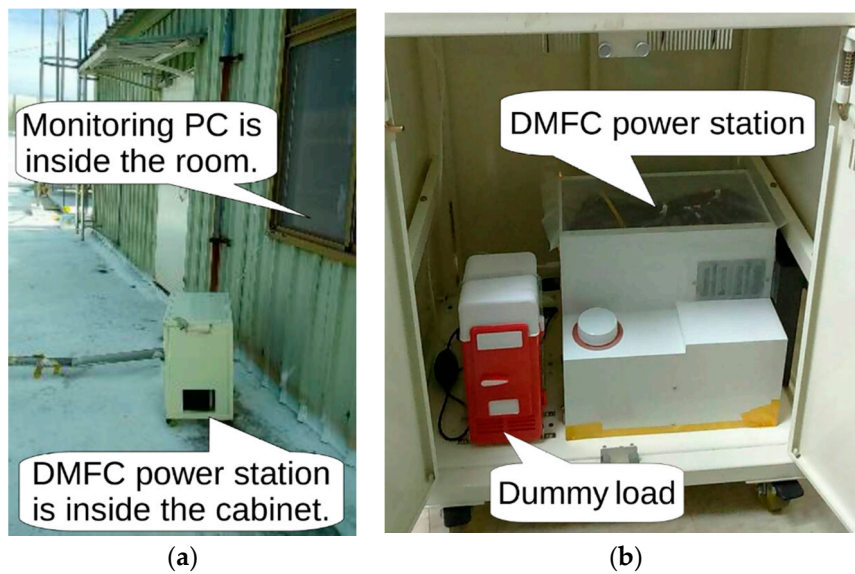


Figure 7. DMFC power station experiment setup. (a) Outside view; (b) inside view.

To test the power station to its full capacity, with 4 stack modules installed, the power generating capability is 3 to 4 W. To guarantee continuous electricity generation at full power for shortening test time, a 10 W thermoelectric cooler was selected as the dummy load. Therefore, P_{Load} was set to 10 W and D_{Load} was set to 1 in the power balance Equation (2), and the battery voltage varied between 3.5 V to 3.7 V due to the EMS over-drainage protection.

4. Results and Discussion

The full 3600 h of long-term outdoor power generation test data are shown in Figure 8. The figure shows the history of temperatures, the variations of stack power generations, and the maintenance events.

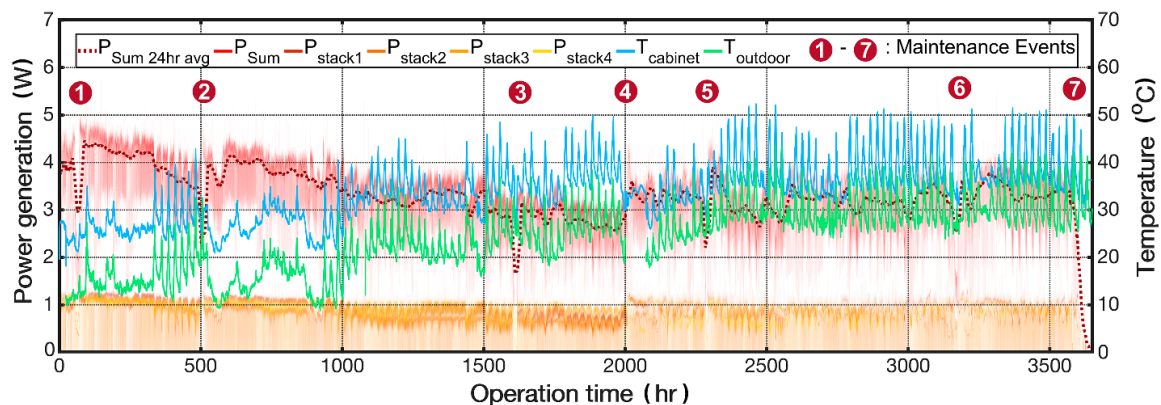


Figure 8. Long-term power-generation test data in an actual outdoor environment.

4.1. Temperature

The temperature outdoors and that inside of the cabinet is shown in green and blue respectively. The temperature inside can be higher by as much as 10–15 °C due to direct sunlight and self-heating by the power station. In the winter, the outdoor temperature fell below 10 °C, while it was always higher than 20 °C inside with the power station in operation except for a short time from a cold start. In the summer, the maximum outdoor temperature reached 40 °C while it rose to 50 °C inside the cabinet.

4.2. Power

The four thin lines in brown, red-orange, yellow-orange, and yellow, at the bottom of Figure 8 represent the power generation of the four stacks, respectively. The power fell to zero periodically as the power generation was suspended for the stack refreshing in the activation state. The theoretical optimal power generation of a single stack was approximately 1 W, and the actual power generation decreased when the reaction temperature deviated to either side from the optimal.

The thin line in red depicts the total power generated, while its 24-h daily moving average is shown by the dark red dotted line. The total power generated reached 4 W at the beginning then decreased gradually down to less than 3 W after hour 1600 when the weather warmed up. In order to compensate for the evaporation of water at high summer temperature, the methanol concentration was reduced to 80 v/v% after hour 2006 from the pure methanol for the winter. The power generation recovered to 3.3 W throughout the rest of the experiment.

4.3. Maintenance

In Figure 8, the sudden changes in the daily power average represented an abnormal event of the power station and they are marked by event numbers in chronological order. Event at hour 55 (❶), the power station suffered a shutdown due to initial wiring mistake. Normal operation resumed after correction. Events at hour 497 (❷), hour 1602 (❸), and hour 2280 (❹) were shutdowns caused by exhaustion of fuel. The power station resumed operation after replenishment. At hour 2006 (❺), the fuel concentration was changed for the summer. Event at hour 3165 (❻) was the first failure when the rusted buckle of dosing pump 2 broke and the deteriorated dosing pump 4 was also replaced. The power station resumed power generation after maintenance. After hour 3581 (❼) the characteristics of 4th stack became abnormal, and the rest of the stacks became flooded and failed subsequently. The power station stopped its operation and concluded the long-term test after hour 3628.

4.4. Failure Analysis

Investigating the episodes resulting in the final failure, Figure 9 zooms in on the records of the four stacks in the range of hour 3581 to 3631. The frames show the voltages, the power generation, and the temperature from top to bottom. The figure shows a normal operation initially in which the power outputs from the stacks were all approximately 1 W, the voltages were controlled at 2.8 V, and the stack temperatures were rising above 55 °C as the ambient temperature rose.

The failure event started to develop at 3582 h into the experiment when the power generation and, thus, also the temperature, of the 4th stack on one side of the station, as shown in yellow, became lower than other stacks. The 4th stack was cut off and shut down because an abnormality was determined by the EMS at hour 3589 (❶) and its voltage peaked briefly and dropped gradually to zero followed by its temperature reaching 7 °C lower than others. It started to sink heat from the others. After hour 3591, the power of the 2nd stack, shown in red-orange, began to oscillate and become frail even though the ambient temperature fell back. At hour 3600 (❷), the 2nd stack got cut off, and stopped generating power causing temperature drops. Since it is sandwiched by the still normal and heat generating stacks 1 and 3, its temperature did not decrease as much as the 4th stack. The power of the 1st stack also became frail, as shown in brown, until it stopped at hour 3606 (❸). At this time, the power generation of the 3rd stack, shown in orange, briefly increased to compensate for the over-cooling temperature, and then finally diminished. At hour 3621 (❹), the researcher came to check and restarted the power station. Although the 1st and 2nd stacks could still be restarted, their powers quickly failed again. The EMS determined that the system could not operate anymore at hour 3628 (❺) and stopped. Based on this final episode, from the first stack power failure to the total shutdown took about 32 h. With multiple stack modules in the system, the redundancies enhanced durability and provided lead time to call for maintenances.

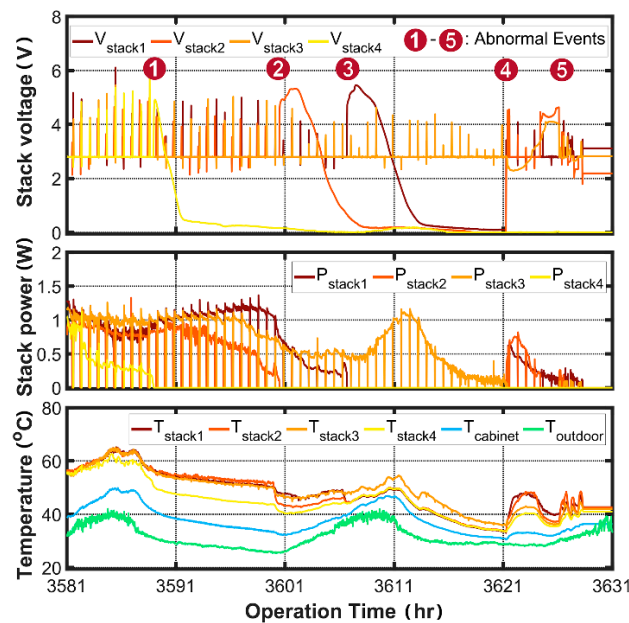


Figure 9. High-resolution experimental record from 3581 to 3631 h.

A forensic engineering study was carried out on the failed stack modules, and the final failure was caused by the aging of MEAs. The degradation of electrochemical efficiency leads to increasing fuel demand at the targeted operating condition beyond MEA capability and successively causing damage by flooding.

4.5. Fault Management

Analyzing the episode of the aforementioned failure events for causes and effects, the design and control logics can be refined for better durability. In the final failure, it commenced when a stack had an abnormality and was turned off, whereby the abnormal stack stopped generating power and started sinking the heat from other stacks causing the EMS to make wrongful judgments that led to other flooding failures successively. While the logic of the aggressive fault tolerant auto-recovery feature is still under development, a conservative fault-management strategy could be preferred during the verification to reduce the risk of chained faults. In the case of any stack failure, just shut down the station, and send a notification of abnormality for forensic investigation, maintenance, and improvements.

4.6. Discussion

The long-term performance of our system was determined from the test record, which is compared with other DMFC systems reported in the literature as shown in Table 1.

In designing the power driving capability, although our semi-active DMFC with 4 stack modules has only rated 4 W, we added Li-ion battery buffering as well as an output regulator to boost intermittent load-driving capability to 12 W. With 12 W, it can drive high-power sensors, actuators, or a wireless device for radio communications. Therefore, the design is suitable for IoT applications. Due to the simplified components and piping, our effective system volume-based energy density reached a comparable 152 Wh/L despite a low 10% electrochemical conversion efficiency and low fuel volume-based energy density of 500 Wh/L. Moreover, due to mechanical compactness in exchange for a larger fuel tank while maintaining portability, 480 h of operating time between refueling is more than 3 times that of other systems under persistent full power demand.

Table 1. Performance specifications of the DMFC generating systems reported in the literature [19,31].

	Generating Power	System Volume-Based Energy	Fuel Volume-Based Energy	Conversion Efficiency	Cartridge Volume and Generating Time
Motorola Lab [32]	2 W	155 Wh/L	956 Wh/L	20%	48 h with 200 cc methanol
LG Chem [33]	25 W	250 Wh/L	1250 Wh/L	26%	10 h with 200 cc methanol
Toshiba [34]	1 W	143 Wh/L	800 Wh/L	16%	20 h with 25 cc methanol
SFC EFOY COMFORT 80i [35]	40 W	163 Wh/L ¹	1100 Wh/L	22%	137.5 h with 5 L methanol
Our system	4 W (output 12 W)	152 Wh/L	500 Wh/L	10%	480 h with 4 L methanol

¹ Consider with M5 fuel cartridge.

This system demonstrated a stable average power generation above 3.3 W throughout the 3600 h of test. With semi-active controls, adjusting the methanol concentration from pure to 80 v/v% helped to improve the power-generation efficiency in hot summer. For the long run, operating characteristics could be updated to reflect the deterioration, or the geometric thermal conditions, so that premature flooding can be avoided and the life can be further extended. To increase power capacity, enlarging the stack for a larger reaction area, increasing the number of stack modules, and improving the reaction efficiency and stability by further optimizing the thermal balance controls are all possible. While increasing the volume energy density for portability, the space utilization of the system can be further polished.

5. Conclusions

A novel portable DMFC power station has been developed for long-term field IoT applications with modularized semi-active stacks and mechatronic controls. Its configuration and controls are introduced in detail. The architecture of the active DMFC stack system was simplified to solve the problems of low manufacturing yield and high maintenance difficulties of active systems. Meanwhile, the EMS was redesigned to achieve coordinated controls on multi semi-active DMFC stack modules to increase configuration flexibility and power capability while overcoming the instability of the passive systems.

The prototype of the power station was tested for 3600 h operation in an actual outdoor environment throughout winter and summer with the ambient temperature ranging from 10 °C to 40 °C and a variety of weather conditions to verify its in-field feasibility and reliability. The causes of the 3 faults were discovered and resolved fundamentally. Therefore, the power station is proven to have long-term outdoor weather endurance, stable power generation, high system volume-based energy density, and easy portability. It is also enhanced with Li-ion batteries buffering and an output regulator to provide an intermittent high-power output drive. Therefore, it is feasible and marketable for remote mobile IoT applications.

Author Contributions: The project was conceptualized by K.-Y.K. and C.-J.C. under the project leadership of L.-D.T. Subsequent methodology development and validation was carried out by C.-J.C., K.-Y.K., and C.-J.L. on the EMS with mechatronics controls and data curation and analysis by C.-J.C. The academic writing was initially drafted by C.-J.C. and S.-B.J. and was later refurbished by C.-J.C. and T.-L.Y. for publication. All authors have read and agreed to the published version of the manuscript.

Funding: This research received no external funding.

Acknowledgments: We thank the Industrial Technology Research Institute of Taiwan for providing the resources, the technology of fuel cells, as well as their supports so that the development and verification was possible.

Conflicts of Interest: The authors declare no conflict of interest.

References

1. Groom, T.B.; Gabl, J.R.; Pourpoint, T.L. Portable Power Generation for Remote Areas Using Hydrogen Generated via Maleic Acid-Promoted Hydrolysis of Ammonia Borane. *Molecules* **2019**, *24*, 4045. [[CrossRef](#)]
2. Chalasani, S.; Conrad, J.M. A survey of energy harvesting sources for embedded systems. In Proceedings of the IEEE SoutheastCon 2008, Huntsville, AL, USA, 3–6 April 2008; pp. 442–447.
3. Shaikh, F.K.; Zeadally, S. Energy harvesting in wireless sensor networks: A comprehensive review. *Renew. Sustain. Energy Rev.* **2016**, *55*, 1041–1054. [[CrossRef](#)]
4. Ko, H.; Lee, J.; Jang, S.; Kim, J.; Pack, S. Energy Efficient Cooperative Computation Algorithm in Energy Harvesting Internet of Things. *Energies* **2019**, *12*, 4050. [[CrossRef](#)]
5. Zareei, M.; Vargas-Rosales, C.; Anisi, M.H.; Musavian, L.; Villalpando-Hernandez, R.; Goudarzi, S.; Mohamed, E.M. Enhancing the Performance of Energy Harvesting Sensor Networks for Environmental Monitoring Applications. *Energies* **2019**, *12*, 2794. [[CrossRef](#)]
6. Wilberforce, T.; Alaswad, A.; Palumbo, A.; Dassisti, M.; Olabi, A.G. Advances in stationary and portable fuel cell applications. *Int. J. Hydrog. Energy* **2016**, *41*, 16509–16522. [[CrossRef](#)]
7. Chen, Y.-S.; Lin, S.-M.; Hong, B.-S. Experimental Study on a Passive Fuel Cell/Battery Hybrid Power System. *Energies* **2013**, *6*, 6413–6422. [[CrossRef](#)]
8. Bajpai, P.; Dash, V. Hybrid renewable energy systems for power generation in stand-alone applications: A review. *Renew. Sustain. Energy Rev.* **2012**, *16*, 2926–2939. [[CrossRef](#)]
9. Lagorse, J.; Paire, D.; Miraoui, A. Sizing optimization of a stand-alone street lighting system powered by a hybrid system using fuel cell, PV and battery. *Renew. Energy* **2009**, *34*, 683–691. [[CrossRef](#)]
10. Alsharif, M. A Solar Energy Solution for Sustainable Third Generation Mobile Networks. *Energies* **2017**, *10*, 429. [[CrossRef](#)]
11. Ellis, M.W.; Von Spakovsky, M.R.; Nelson, D.J. Fuel cell systems: Efficient, flexible energy conversion for the 21st century. *Proc. IEEE* **2001**, *89*, 1808–1818. [[CrossRef](#)]
12. Velisala, V.; Srinivasulu, G.N.; Reddy, B.S.; Rao, K.V.K. Review on challenges of direct liquid fuel cells for portable application. *World J. Eng.* **2015**, *12*, 591–606. [[CrossRef](#)]
13. Carrette, L.; Friedrich, K.; Stimming, U. Fuel cells—fundamentals and applications. *Fuel Cells* **2001**, *1*, 5–39. [[CrossRef](#)]
14. Zhang, T.; Wang, Q.-M. Performance of miniaturized direct methanol fuel cell (DMFC) devices using micropump for fuel delivery. *J. Power Sources* **2006**, *158*, 169–176. [[CrossRef](#)]
15. Das, V.; Padmanaban, S.; Venkitesamy, K.; Selvamuthukumar, R.; Blaabjerg, F.; Siano, P. Recent advances and challenges of fuel cell based power system architectures and control—A review. *Renew. Sustain. Energy Rev.* **2017**, *73*, 10–18. [[CrossRef](#)]
16. Kuan, Y.-D.; Lee, S.-M.; Sung, M.-F. Development of a Direct Methanol Fuel Cell with Lightweight Disc Type Current Collectors. *Energies* **2014**, *7*, 3136–3147. [[CrossRef](#)]
17. Zhu, Y.; Liang, J.; Liu, C.; Ma, T.; Wang, L. Development of a passive direct methanol fuel cell (DMFC) twin-stack for long-term operation. *J. Power Sources* **2009**, *193*, 649–655. [[CrossRef](#)]
18. Achmad, F.; Kamarudin, S.K.; Daud, W.R.W.; Majlan, E.H. Passive direct methanol fuel cells for portable electronic devices. *Appl. Energy* **2011**, *88*, 1681–1689. [[CrossRef](#)]
19. Kamaruddin, M.Z.F.; Kamarudin, S.K.; Daud, W.R.W.; Masdar, M.S. An overview of fuel management in direct methanol fuel cells. *Renew. Sustain. Energy Rev.* **2013**, *24*, 557–565. [[CrossRef](#)]
20. Sgroi, M.; Zedde, F.; Barbera, O.; Stassi, A.; Sebastián, D.; Lufrano, F.; Baglio, V.; Aricò, A.; Bonde, J.; Schuster, M. Cost Analysis of Direct Methanol Fuel Cell Stacks for Mass Production. *Energies* **2016**, *9*, 1008. [[CrossRef](#)]
21. Kamarudin, S.K.; Achmad, F.; Daud, W.R.W. Overview on the application of direct methanol fuel cell (DMFC) for portable electronic devices. *Int. J. Hydrog. Energy* **2009**, *34*, 6902–6916. [[CrossRef](#)]
22. Li, X.; Faghri, A. Review and advances of direct methanol fuel cells (DMFCs) part I: Design, fabrication, and testing with high concentration methanol solutions. *J. Power Sources* **2013**, *226*, 223–240. [[CrossRef](#)]
23. Marx, N.; Boulon, L.; Gustin, F.; Hissel, D.; Agbossou, K. A review of multi-stack and modular fuel cell systems: Interests, application areas and on-going research activities. *Int. J. Hydrog. Energy* **2014**, *39*, 12101–12111. [[CrossRef](#)]

24. Vulturescu, B.; De Bernardinis, A.; Lallemand, R.; Coquery, G. Traction power converter for PEM fuel cell multi-stack generator used in urban transportation. In Proceedings of the 2007 European Conference on Power Electronics and Applications, Aalborg, Denmark, 2–5 September 2007; pp. 1–10.
25. Cardozo, J.; Marx, N.; Boulon, L.; Hissel, D. Comparison of Multi-Stack Fuel Cell System Architectures for Residential Power Generation Applications Including Electrical Vehicle Charging. In Proceedings of the 2015 IEEE Vehicle Power and Propulsion Conference (VPPC), Montreal, QC, Canada, 19–22 October 2015; pp. 1–6.
26. Wu, C.-C.; Chen, T.-L. Dynamic Modeling of a Parallel-Connected Solid Oxide Fuel Cell Stack System. *Energies* **2020**, *13*, 501. [[CrossRef](#)]
27. Yang, C.-H.; Chang, S.-C.; Chan, Y.-H.; Chang, W.-S. Dynamic Analysis of the Multi-Stack SOFC-CHP System for Power Modulation. *Energies* **2019**, *12*, 3686. [[CrossRef](#)]
28. Hu, X.; Wang, X.; Chen, J.; Yang, Q.; Jin, D.; Qiu, X. Numerical Investigations of the Combined Effects of Flow Rate and Methanol Concentration on DMFC Performance. *Energies* **2017**, *10*, 1094. [[CrossRef](#)]
29. Kim, Y.; Shin, D.; Seo, J.; Chang, N.; Cho, H.; Kim, Y.; Yoon, S. System integration of a portable direct methanol fuel cell and a battery hybrid. *Int. J. Hydrog. Energy* **2010**, *35*, 5621–5637. [[CrossRef](#)]
30. Leo, T.; Raso, M.; Navarro, E.; Mora, E. Long Term Performance Study of a Direct Methanol Fuel Cell Fed with Alcohol Blends. *Energies* **2013**, *6*, 282–293. [[CrossRef](#)]
31. Zhao, T.S.; Yang, W.W.; Chen, R.; Wu, Q.X. Towards operating direct methanol fuel cells with highly concentrated fuel. *J. Power Sources* **2010**, *195*, 3451–3462. [[CrossRef](#)]
32. Xie, C.; Bostaph, J.; Pavio, J. Development of a 2W direct methanol fuel cell power source. *J. Power Sources* **2004**, *136*, 55–65. [[CrossRef](#)]
33. LG Chem commercializes portable fuel cell. *Fuel Cells Bull.* **2005**, *2005*. [[CrossRef](#)]
34. Latest DMFC prototypes from Toshiba, Hitachi. *Fuel Cells Bull.* **2003**, *2003*. [[CrossRef](#)]
35. EFOY COMFORT Technical Data. Available online: <https://www.efoy-comfort.com/technical-data> (accessed on 1 March 2020).



© 2020 by the authors. Licensee MDPI, Basel, Switzerland. This article is an open access article distributed under the terms and conditions of the Creative Commons Attribution (CC BY) license (<http://creativecommons.org/licenses/by/4.0/>).